Design and Assessment of a Super-High Speed, Hybrid Hydrofoil/SWATH Crew Boat

Author Names: Vasileios Georgiadis, Kyle Miller, and Leon Faison
Completed at the Innovative Ship Design Lab, Massachusetts Institute of Technology

ABSTRACT

The need to expeditiously transfer personnel from shore to oil platforms exists within the offshore oil industry. A concept design for a high-speed vehicle called Wavecutter is proposed as a solution and assessed. Wavecutter is a hybrid design that would combine the advantages of a SWATH design with those of surface-piercing (SP), super-cavitating (SC) hydrofoils. In high sea states, the vessel travels at lower speeds in displacement mode, taking advantage of the seakeeping characteristics of the SWATH design. At lower sea states, the vessel will travel in excess of 80 knots in foil borne mode, taking advantage of the high lift to drag ratio of the hydrofoils. The hydrofoil design began with preliminary weight estimations and calculations of the lift forces needed to support the vessel in foil borne mode. Sizing and foil profile considerations were examined based on the speed profile determination. A feasibility assessment was then conducted on the hydrofoils by determining the structural loading and stress response. A hybrid SP-SC hydrofoil, based on a new SC section blended with a partial NACA 4412 section was designed and chosen as the preferred type of hydrofoil for this craft. Finally, static stability and seaworthiness in head waves was evaluated at maximum speed. The vessel demonstrated positive longitudinal static stability and acceptable seakeeping behavior. Future studies should focus on CFD seakeeping analysis, global structural analysis, and determination of an exact seakeeping operational safety envelope. Overall, Wavecutter presents a viable option for super-high speed crew transport comparable to other means of transportation.

INTRODUCTION

The motivation for this design is to create an improved vessel for rapid crew and/or small goods transportation from harbors to offshore installations. Different designs of semi-displacement vessels (largest units) or planing crafts (smallest) dominate the current method of transportation. The maximum speed reached by planing hulls is in the range of 50-55 knots in calm seas, while speed rapidly falls below 20 knots in moderate sea states. Few hydrofoil vessels have been built to reach speeds of higher than 60 knots. One of the most successful designs is made by Boeing, called Jetfoil, which uses fully submerged foils. This design requires complex control mechanisms with very fast reaction times at speeds in excess of 80 knots. These types of hydrofoil crafts switch to displacement mode when encountering heavy weather. For transportation service of goods and crew that require speeds above 70 knots, one must use helicopters. These vehicles are very sensible to change in weather conditions and very limited in payload capacity.

In order to provide better operability in a wider range of weather conditions and proper payload efficiency with very-high speed to station, innovative hull designs and features have been considered. The new design would need to incorporate features that provide both good seakeeping characteristics along with the ability to travel at high speeds. Design requirements were determined based on existing vessels used for the same purpose. The speed range requirement was defined based on the desired maximum speed but also with knowledge of expected speed limitations of hydrofoil vessels. The Gulf of Mexico, home to numerous offshore oil platforms, was used to derive the endurance and sea state requirements. The endurance requirement was based on the distance of the furthest oil rig from the Gulf's main harbor. The sea state requirement was derived by analyzing sea statistics specific to the Gulf of Mexico [1]. The final design requirements are shown in Table 1.

Table 1: Design Requirements

Requirement	Objective	Threshold
Passengers	24	20
Cargo [MT]	15	10
Crew	4	6
Max Speed [kts]	85	70
Endurance [nm]	600	400
Operational Sea State[1]	4 (upper bound)	3 (upper bound)

WAVECUTTER CONCEPT DESIGN

The concept design of the vessel was based on Dr. Brizzolara's autonomous unmanned hybrid concept design [2]. This novel patented[2] technology combines the superior seakeeping ability of an unconventional SWATH design in higher sea states with surface piercing hydrofoils to achieve higher speeds in milder sea states. The ultra-high speed SWATH with hydrofoil design establishes two modes of operation. At slower speeds, less than 20 knots, the vessel travels in displacement mode, where the SWATH design takes advantage. As the vessel moves into the higher speed regime, hydrodynamic forces take over and the vessel begins to lift out of the water until it is stabilized on four surface piercing hydrofoils. In the transition phase, hydrofoils are rotated to be parallel with the water level, providing maximum lift for the given speed. As the vessel lifts, the hydrofoils rotate outwardly into the water until a dihedral angle of 40 degrees from the water level is achieved. The two modes along with the transition phase for *Wavecutter* are shown in Figures 1-3 below.

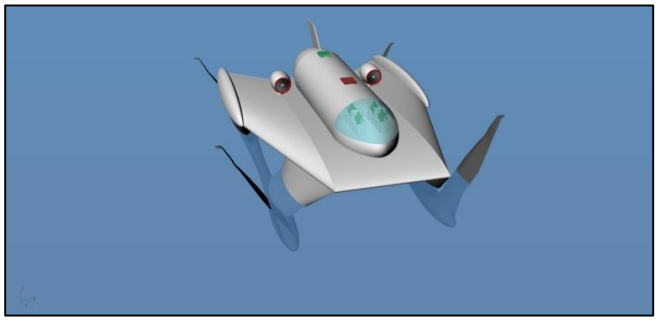

Figure: 1 Displacement Mode

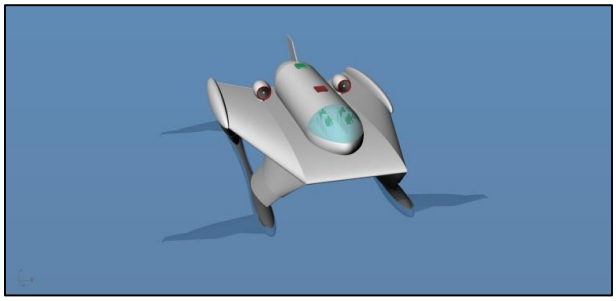

Figure 2: Transition Phase

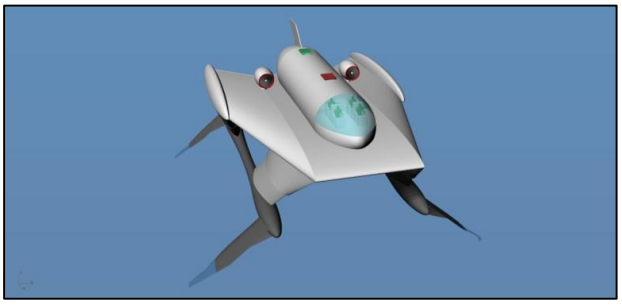

Figure 3: Foil Borne Mode

The vessel's primary components and propulsion system are shown in Figures 4 and 5 respectively. In displacement mode, power is generated from the diesel generator set, and transmitted to the propeller by a frequency controlled electrical motor. The engines providing propulsion in foil borne mode are turbofan aircraft engines, located on either side of the manned module on top of the wing. To select the diesel generator set, the resistance has been estimated in displacement mode for a speed of 17 knots. The resistance estimations in displacement mode are based on Dr. Brizzolara's total resistance comparison of unconventional SWATH hulls with different slenderness ratios and volumetric Froude numbers [3]. The volumetric Froude number is based on the SWATH hull displaced volume.

$$Fn_v = \frac{V_{ship}}{\sqrt{g * \nabla^{(\frac{1}{3})}}} = 1.127$$

$V_{ship} = 17\ knots$

$\nabla = 245.52\ m^3, total\ diplaced\ volume$

The total resistance is

$$R_t = C_{T\nabla} * \frac{1}{2} * \rho * {V_{ship}}^2 * \nabla^{\frac{2}{3}} = 123\ KN$$

$C_{T\nabla} = 0.08, total\ resistance\ volumetric\ coefficient$

$$Effective\ Horsepower\ (EHP)[KW] = Resistance[KN] * Speed\left[\frac{m}{s}\right]$$

[1] Sea State defined per NATO standards

[2] US Patent pending 20120192781-A1.

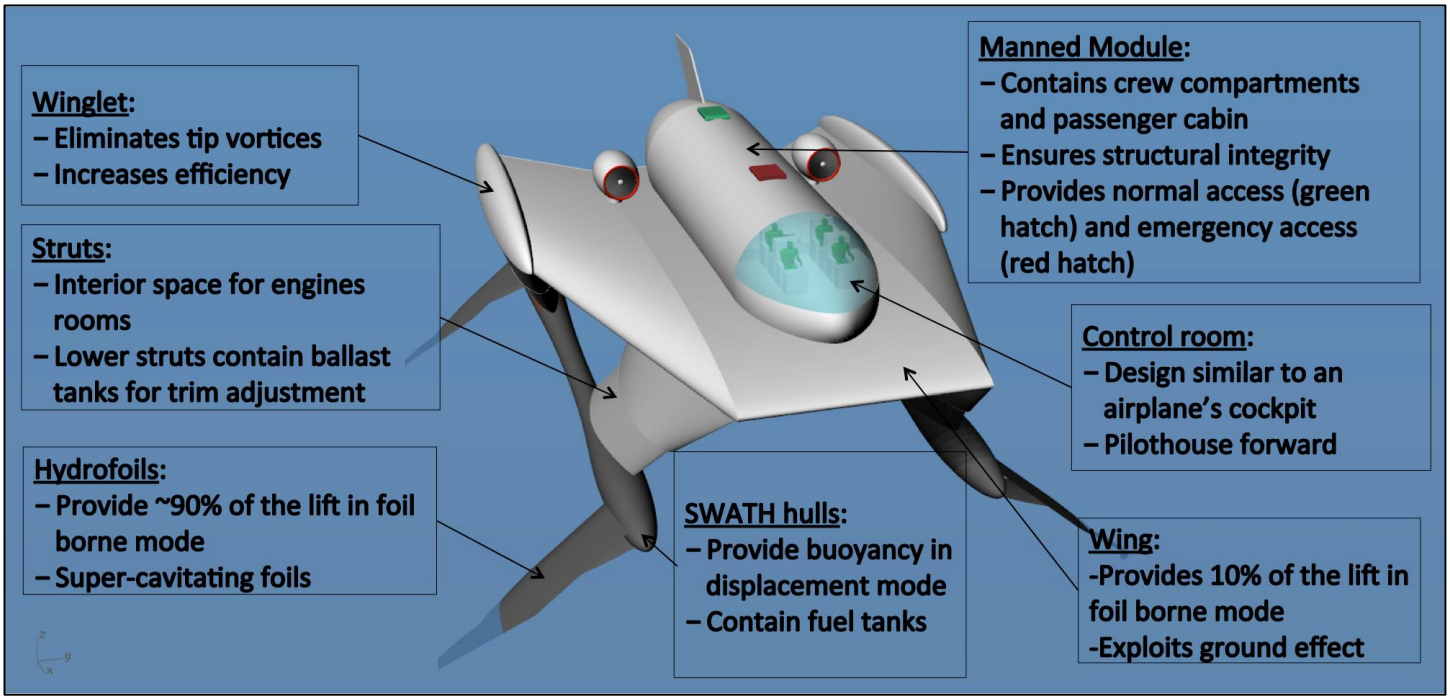

Figure 4: Vessel Components

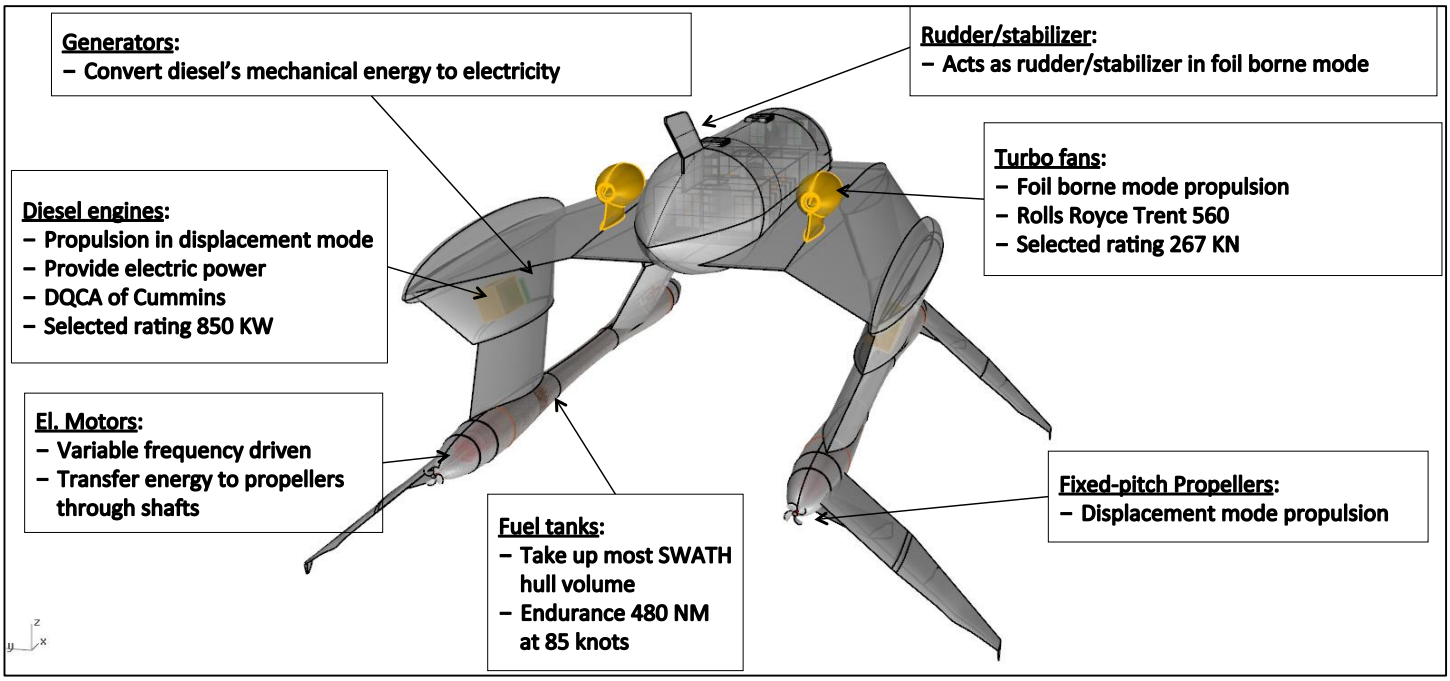

Figure 5: Propulsion System

Using estimated propulsive, mechanical and electrical efficiency coefficients, the brake horsepower (BHP) can be calculated, as shown in Table 2. A Cummins DQCA 60 Hz Diesel Generator Set rated at 850 kW was selected.

Table 2: Resistance Calculations

EHP [KW]	1076	Maximum speed with Diesel [m/s]	8.75
SHP [KW]	1435	Propulsive coefficient (P.C.)	0.75
BHP [KW]	1511	Mechanical Efficiency	0.95
Required power of Diesel Engines KW]	1679	Electrical efficiency	0.9
Number of Engines	2	Required power per engine [kW]	840

The calculation of the required power at maximum speed is based on the estimated total resistance of the drag in water and in air. The drag in water imposed on the hydrofoils is based on empirical data extrapolated from model test data [4]. Drag in air is based on semi-empirical formulas for low aspect ratio wings, obtained from Hoerner [5]. The final design distribution of drag components at maximum speed can be seen in Figure 6. It can be seen from the figure that air drag is a small portion of the total drag. The total drag is 483 kN. Adding a rough sea allowance of +10%, the total drag becomes 532 kN. Thus, each turbofan engine must provide at least 266 KN.

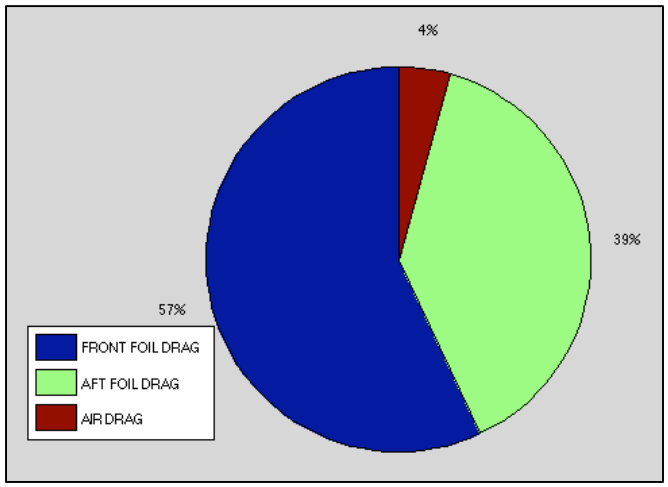

Figure 6: Total Drag Force Distribution at Maximum Speed (Equilibrium Condition)

The engine database for turbofan selection was the Trent series of Rolls-Royce, because it was the most open source database found. The engine selected is Trent 560, currently used in airplanes Airbus 340-600. The ratings and characteristics are shown below.

Table 3: Selected Turbo-fan Engine Characteristics

Engine	Trent 560
Entry Into Service	2002
Applications	Airbus A340-600
Static Thrust [KN]	266.89
Basic Engine Weight [kg]	4717.36
Thrust to Weight Ratio	5.76
Length [m]	3.91
Fan Diameter [m]	2.47

A recognized technical risk of this design is the placement of airplane turbo fans close to the sea water surface level. Corrosion problems that may arise due to the salt deposits on the blades may be significant, if not properly addressed with a “marinized” design.

The initial design loop revealed that the main driver of the displacement is fuel (~35% of total displacement with 600 NM endurance) and the hydrofoils (~25% of total displacement) but from solid high strength metal alloy. In the final design loop, the best compromise between endurance, maximum speed and required power amounted to a fuel amount enough for 480 NM endurance (at maximum speed).

Internal arrangements design focuses on manned compartments. Normally, in a large naval vessel there is a control room, from where the crew members control and monitor the vessel’s systems. There is also a need for a navigation room, from where a visual appreciation of the surroundings will be possible. To keep consumed space low, these two rooms were combined into a single control room, which has been placed in the front part of the wing. There is also a need for crew office space, and an emergency berthing room. All these spaces are allocated in a common compartment behind the control room compartment. The emergency berthing room will be used for medical emergencies, as well as a resting place for the crew member who will perform watch duty while at harbor. A visual depiction of the manned space is found in Figure 7.

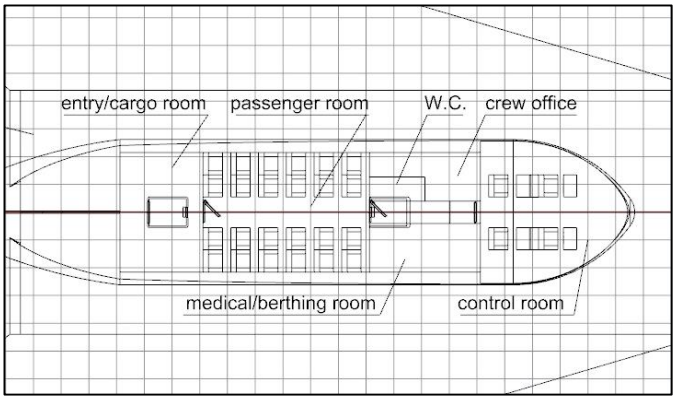

Figure 7: Manned Nacelle Space Allocation

Overall, the required payload of *Wavecutter* resulted in a different design spiral than the unmanned design of Brizzolara [2]. The main dimensions of *Wavecutter* are seen in the three figures below (all dimensions are in m). The blue line in the figures represents the water level at maximum speed.

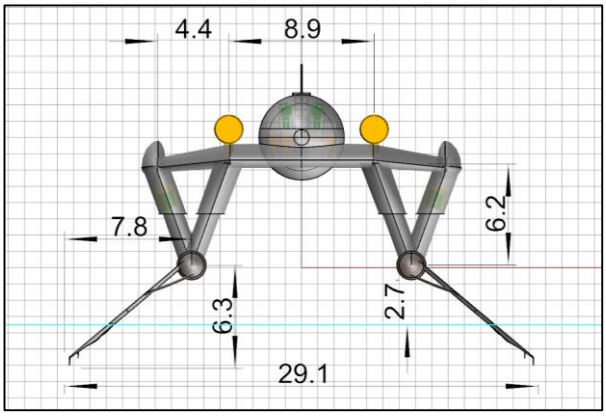

Figure 8: Front View Vessel Dimensions

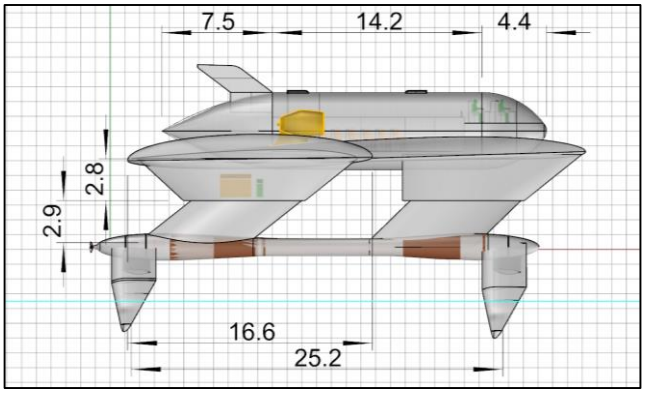

Figure 9: Profile View Vessel Dimensions

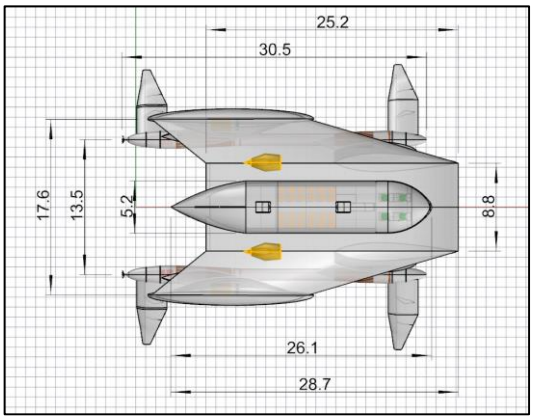

Figure 10: Top View Vessel Dimensions

The very fact that *Wavecutter* is manned dictates special attention to safety. Structural analysis and support options for the hydrofoils is of the utmost importance, since rupture of a hydrofoil is likely to result in dangerous motions of the vessel. Another important consideration is the risk capsizing, which is why stability is on the list of feasibility assessments. In addition, seakeeping and dynamic behavior in general are topics that require much more attention than they would in an unmanned vessel, which is why they are a major priority of the feasibility assessment phase of this study.

HYDROFOIL DESIGN

The general design of the vessel is followed by the hydrofoil design, presented in this section and pictured in Figure 18. The new hydrofoil introduced by Brizzolara [6] is special for two reasons. First, it is a super-cavitating hydrofoil (SC), and this allows the hydrofoil to optimally provide lift above cavitation speeds (approximately above 50 knots). Second, unlike typical SC hydrofoils, its unique optimized profile solves the unsteady ventilation problem[3]. The latter has been proven by CFD simulations [6] and model experiments [4]. The capability of this profile to retain steady ventilation areas even under unsteady conditions (of certain bounds) is crucial, because it allows prediction of lift and drag under unsteady flow conditions. Figure 11 shows a 3D view of the hydrofoil. Figure 12 shows the basic profile shape designed by Dr. Brizzolara and analyzed with 2D CFD simulations performed in unsteady turbulent cavitating flow conditions; inflow is right to left, gasous cavity is presented in blue, water in red. Note that in Figure 12 the leading edge is on the right.

[3] The air cavity in surface piercing hydrofoils is different than that in fully submerged hydrofoils under fully cavitating conditions: a great portion of the air is drawn from above the water surface. This often causes unsteadiness in the ventilated area of surface piercing foils.

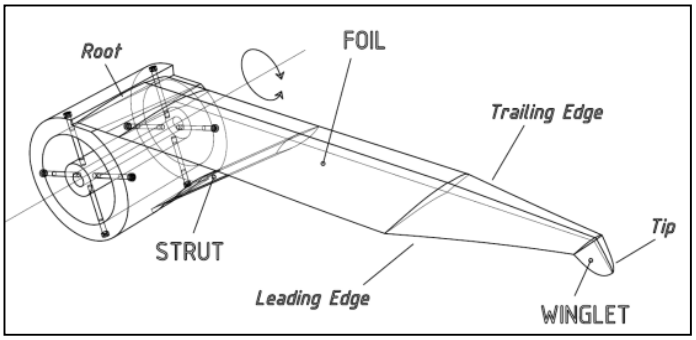

Figure 11: 3D SC-SP Hydrofoil design

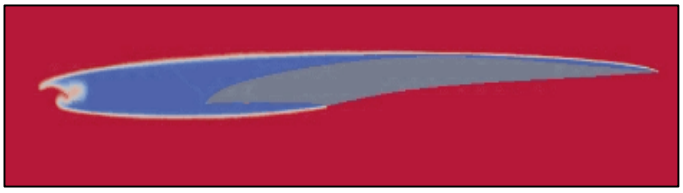

Figure 12: Unsteady Turbulent Flow Simulation

Hydrofoil forces estimations have been made through data analysis of the measurements provided by the model experiments on a 3D hydrofoil [4], designed by means of a reformulated lifting line theory valid for surface piercing supercavitating profiles [7].

Several assumptions are made in order to make this leap from model to full scale. First, it has been assumed that geometric similitude is sufficient to allow equating the coefficients of force to be equal, model to full size hydrofoil, in the same normalized submerged length and angle of attack. Second, it is assumed that scaling up the model hydrofoil will retain its capability to ventilate steadily even under unsteady conditions. Third, it is assumed that cavitation number does not play a significant role in the full scale hydrofoil for angles of attack[4] between -3 and 8. This was evident in the model experiments' results [4] and the same is assumed for the full scale hydrofoils. It is recognized that Froude and Reynolds number similitude was not achieved between the model and full scale foil. Doing so would not allow the distinct geometrical features of the design to be transferred to the model (the model size would be too small). Froude number and/or Reynolds number do have an effect, but the extent of this effect could not be quantified from the model test campaign, which concentrated on the angle, submergence and cavitation number effects. The effect of Froude number on the dynamic forces of the surface piercing hydrofoil due to wave generation on the free surface is very important up to Fn_c=1[5]. For Fn_c>1, which is the case for Wavecutter at maximum speed, the Froude number effect is related to ventilation, but for this specific hydrofoil design its influence is very limited. Reynolds scale effects are expected to influence the viscous drag part which is a small portion of the total for super-cavitating hydrofoils and even less significant for the lift force. This partially justifies the assumption to neglect Reynolds and Froude scaling effects on the experimental measurements.

The model experimental data contained several measurements of forces and moments, relative to various angles of attack, for three different submerged lengths [4]. Each submerged length was one set of experiments (black curves in Figure 13) with different angles of attack and cavitation numbers, obtained by varying the static pressure inside the cavitation tunnel. The functions of the force coefficients relative to the submerged length and angle of attack have been obtained through polynomial interpolation between the three different sets of experiments. The resulting surface in 3D space for the lift coefficient is shown in Figure 13. In this Figure, the x axis represents the submerged length, the y axis the angle of attack and the z axis the lift coefficient. Surface bounds correspond to the valid prediction range; outside these bounds the results of this study do not apply. To obtain the hydrofoil forces, the following formulas were used.

$$C_{F_i} = \frac{F_i}{\frac{1}{2} * \rho_{water} * u^2 * A_{foil}} \, , i = 1,2,3$$

The water density ρ_{water} did not change during the experiments. Also the flow speed u was equal to 9 m/s, and remained constant. The submerged hydrofoil area A_{foil} changed in every different set of experiments, because the submerged length changed. The submerged length took the values 175mm, 250mm and 350mm for each set respectively. The formula used to calculate the submerged area is seen below.

$$A_{foil} = 0.1768 * (L_{sub})^2 + 0.0613 * L_{sub}$$

Where
$L_{sub}: submerged\ length\ in\ m$
$A_{foil}: submerged\ area\ in\ m^2$

[4] Wherever angle of attack is mentioned in this section, pitch equivalent angle of attack is meant. Pitch equivalent angle of attack is equal to the angle of attack divided by the sinusoid of the dihedral angle of the foil.

[5] In this case the Froude number (Fn_c) is calculated based on the mean wetted chord of the hydrofoil.

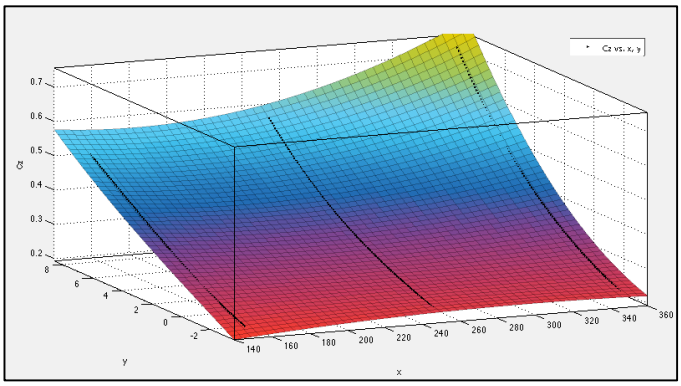

Figure 13: Hydrofoil Lift Force Coefficient response surface with respect to submergence and angle of attack

The hydrofoils need to be sized appropriately for this vessel, based on certain requirements. The first requirement is equilibrium and zero trim at maximum speed. The second is to have sufficient clearance distance from the SWATH hulls to avoid slamming. The last is the size constraint imposed by the folding mechanism of the foils.

The first is satisfied by applying the three equations of equilibrium; the sum of forces and moments must be zero.

$$\sum (F_i)_x = 0$$
$$\sum (F_i)_z = 0$$
$$\sum M_i = 0$$

The vessel's free body diagram in the vertical plane is shown below, along with the reference coordinate system.

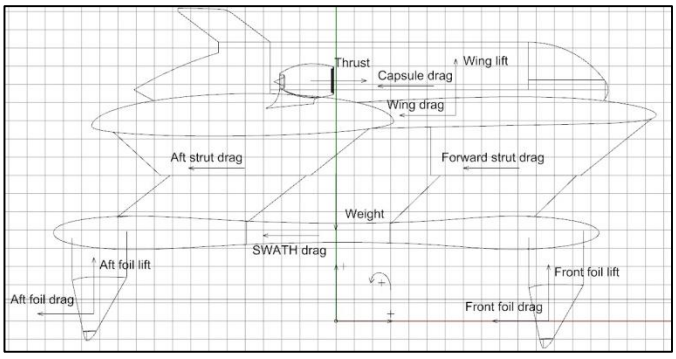

Figure 14: Vessel Free Body Diagram

In the system of equilibrium equations, five forces are unknown: front foils lift, aft foils lift, front foils drag, aft foils drag and thrust. Considering the fact that foil drag and lift are both dependent on submerged foil length and angle of attack, the five unknowns in practice are:

1. Front foil submerged length
2. Aft foil submerged length
3. Front foil design angle of attack
4. Aft foil design angle of attack
5. Thrust

To obtain a unique solution to the system, two of the unknowns need to be defined prior to solving the equations. This is a design decision. Any two of these five factors can be defined to give a different unique solution to the system. It was decided to define the design angles of attack to be zero at equilibrium, at maximum speed. Zero angle of attack in this context means that the design angle of attack of the model hydrofoils is adopted, without change. The choice of keeping the design angle of attack of the hydrofoils is made in order to avoid the following:

- Extrapolating (predicting outside the bounds) of experimental data.
- Large curvatures and values found in the force coefficients near large positive angles of attack.
- Unstable ventilation phenomena at large negative angles of attack influenced by cavitation number.

Thus the angles have been defined and a solution to the system can be obtained. The unique[6] solution to the equilibrium equations is:

1. Front foil submerged length=3460.6 mm
2. Aft foil submerged length=2777.8 mm
3. Thrust=483.43 KN

We notice that the required submerged length of the front foils is larger than that of the aft foils by approximately 25%. Figure 15 shows the moment distribution, at maximum speed in equilibrium condition. Due to the placement of the propulsion system high in the deck, the moment generated by the thrust force is large. To counteract this moment a great contribution is required by the forward foils. The weight lift distribution is shown in Figure 16.

[6] Because the experimental equations used to define foil lift and drag forces are non-linear high order polynomials, many other solutions of the system exist. The one that has the minimum positive values for the three parameters has been selected, which is also the only solution that is physically feasible.

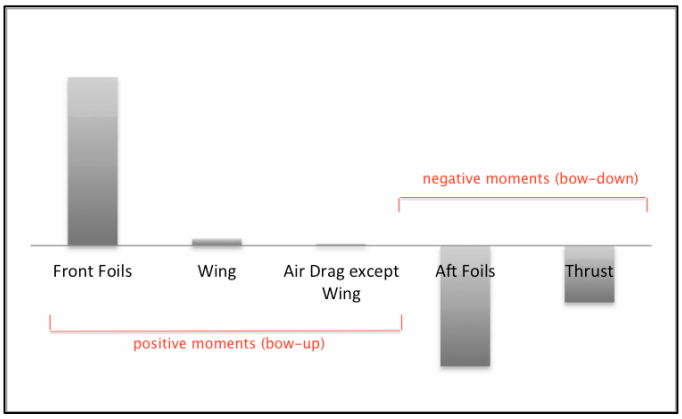

Figure 15: Moment Distribution

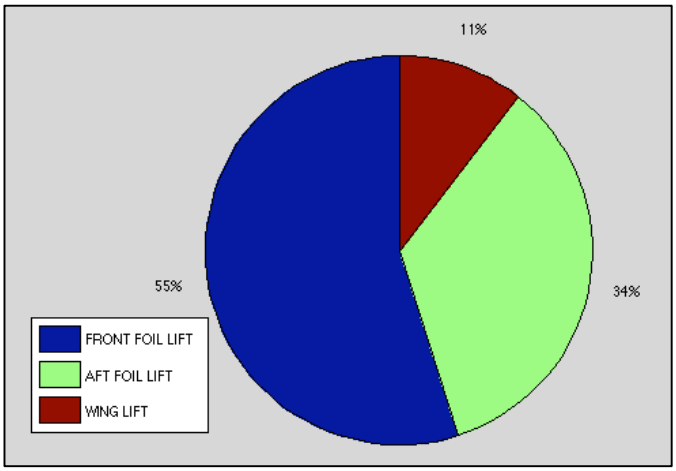

Figure 16: Weight Lift Contribution

Another consideration is the clearance distance from the SWATH hulls (Figure 17). The larger the foil, the less the possibility of water slamming to the SWATH hulls. The clearance distance can be obtained from the following formula.

$$clearance = (total\ length - sub.\ length - S.\ hull\ radius) * \sin(dih.\ angle)$$

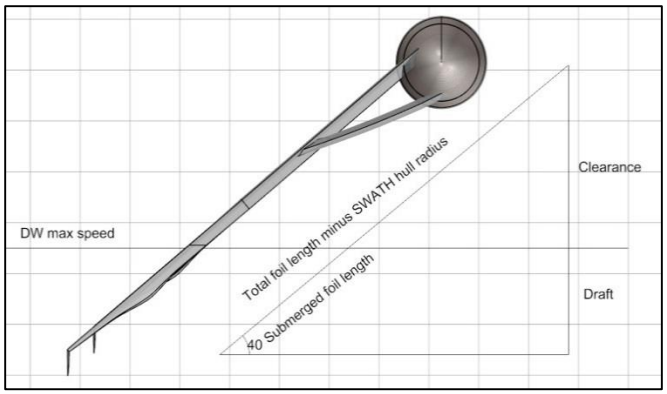

Figure 17: Clearance from SWATH hulls at Max Speed

With a wave height of 2.5 m (upper threshold for the vessel's operational sea state) and an allowance (+10%), a required clearance of 2.8 m is found. This means a total length of ~8.7 m for the front foil and ~8 m for the aft foils. Another design constraint is dictated by the foil folding mechanism's longitudinal length limitation. The folding mechanism cannot be longer than 3 m, therefore the foil span cannot be longer than 3 m. This is why part of the foils are parallel and part of them are tapered. The final sizing of the hydrofoils is shown in Figure 18.

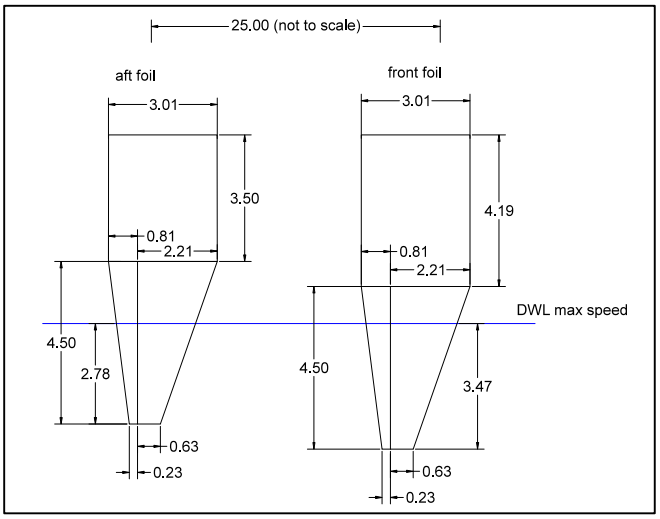

Figure 18: Hydrofoil Sizing (all lengths in m)

HYDROFOIL STRUCTURAL ANALYSIS

Once the size and shape of each hydrofoil was determined for *Wavecutter*, a structural analysis was required due to the long, thin nature of the chosen surface piercing hydrofoils. The design team suspected that structural modifications would be required in order to ensure adequate strength for the hydrofoils. Therefore, the overarching goal of the structural analysis was to determine a way to adequately strengthen the existing hydrofoils while also minimizing the negative effects to the lift and drag forces.

Loading Forces Calculation

The first step in the structural analysis was to determine what type of loading conditions the hydrofoils would encounter during operations. Since *Wavecutter* employs surface piercing hydrofoils, the maximum bending stresses seen by the hydrofoils occur at the interface between the hydrofoil and the SWATH hull. The steady state maximum speed bending force supplied by each of the hydrofoils was calculated from the lift and drag

requirements found in the hydrofoil sizing section of this research.

In addition to the steady state maximum speed loads, reference [8] states that fully submerged hydrofoil systems passing through a seaway are subject to loads induced by waves. The proportional change in foil load due to incoming waves is defined for a fully submerged hydrofoil as:

$$\frac{\Delta L}{L} = \frac{\Delta C_L}{C_L} = \propto_e * \frac{C_{L_\propto}}{C_L}$$

Where:

$$\propto_e = \frac{V_W}{V_S} = \frac{\text{vertical component of wave particle velocity}}{\text{ship's speed}}$$

$C_L: lift\ coeffient$

$C_{L_\propto}: derivative\ of\ lift\ coefficient\ with\ respect\ to\ angle\ of\ attack$

Due to lack of similar estimates for surface piercing hydrofoils, the above equation was then applied to *Wavecutter* in order to approximate added forces due to waves. Assuming a 1.25 m wave amplitude and wave length twice the length between the foils (longitudinal), trochoidal wave theory predicts V_W to be 0.9 m/s for the foil at a depth of 3.47 m. $C_{L_\propto}$ and C_L were found to be 0.03 and 0.3 for this super-cavitating hydrofoil in previously conducted model testing [6]. Using these assumptions and adding the result to the steady state lift forces at maximum speed, the total forces seen by the hydrofoils were calculated. The results are found in Table 4.

Table 4: Hydrofoil Design Forces

	Aft Foil	**Forward Foil**
Total Load [KN]	549	858

Development of the Safety Factor

The design team realized that simply designing a hydrofoil capable of withstanding the forces calculated above is not adequate. Safety factors were necessary in order to ensure the hydrofoils of *Wavecutter* were strong enough to withstand the strong vibrations, corrosion, and unexpected forces usually associated with operations in the marine environment. Unfortunately, a safety factor for hydrofoil structural adequacy was not designated within the DNV/GL or ABS classification society rules. Although these societies specify stress safety factors for the supporting ship structure of hydrofoils, they do not specify any type of factor for the foils themselves.

In the absence of a safety factor guide in the hydrofoil design industry, the aircraft wing and propeller design industries were used for reference. DNV/GL rules specify structural safety factors of 1.6-2.2[7] for different types of propeller blades for high speed craft and the FAA (Federal Aviation Administration) specifies a structural safety factor of 1.5[8] for aircraft wings of transport aircrafts weighing over 6.2 tonnes.

A design safety factor of 2 was chosen for Wavecutter's hydrofoils. Because failure of aircraft wings impacts human safety more than failure of hydrofoils in hydrofoil crafts, this safety factor choice may seem conservative. However, it should be taken into account that this is a preliminary design, where configurations and calculations are approximate. If the safety factor is reduced at later stages of design, the design of the hydrofoils can still be kept the same (with a negative effect on cost of course). However, the opposite is not true: increasing the safety factor later will require a re-design of the hydrofoils.

Structural Design and Analysis Overview

Due to the complex shape of the hydrofoil, computational methods were required to analyze the structure's stress field. In particular, a Finite Element Analysis (FEA) program called Scan&Solve® [9] was utilized. For validations, the results were compared with an analytical maximum stress calculation. In the analytic approach, the hydrofoil is simplified to the shape of a cantilevered beam with equivalent dimensions. The iterative design process was conducted as follows:

[7] DNV/GL HSLC rules Pt. 4 Ch.5

[8] FAA FAR Part 25 (Subpart C)

1. Supporting structure was added to the non-supported hydrofoil, seen in Figure 19, in the Computer Aided Design (CAD) program, Rhino®.

Figure 19: Forward Hydrofoil without Supporting Structure

2. The hydrofoil with the supporting structure was analyzed using the FEA tool Scan&Solve® [9].
3. Refinements to the supporting structure were made until the stresses seen in the hydrofoil were lower than 2X the yield strength of the chosen material.
4. Finally, an estimated maximum stress was calculated for each configuration by approximating the hydrofoil as a cantilevered beam. This estimate was used to compare with the FEA results.

The subsequent sections describe the setup of the hydrofoil model within the FEA program as well as configurations to the supporting structure that were analyzed in this study and their effects on the performance of *Wavecutter*.

Boundary Conditions, Load Placement, and Material

The inner surface of the hydrofoil bearing was chosen as a boundary condition and restrained from moving in all directions, as shown in Figure 20. The design team assumed that this surface would be locked into place by the large machinery needed to rotate the hydrofoil around the strut, thereby making it a reasonable place to position the FEA restraints.

The design forces calculated earlier were applied to the below waterline, underside face of the wetted section of the supercavitating hydrofoil. A visual depiction of these forces being applied to the surface is shown in Figure 20.

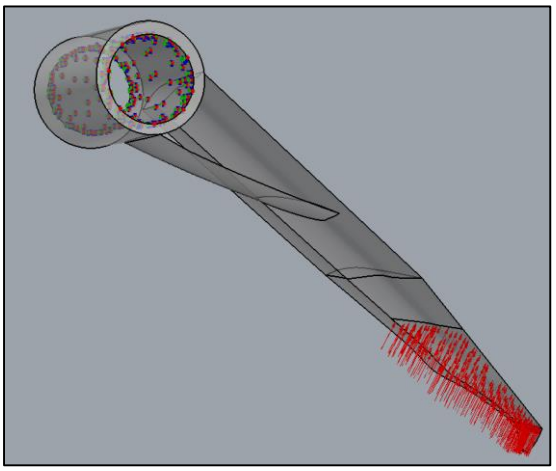

Figure 20: Design Loads and Restraints Applied to Hydrofoil Surfaces (Red Arrows Indicate Force Vectors and Multi-Colored Dots Indicate Restraints.)

A high strength steel with a tensile yield strength of 660 MPa, an elastic modulus of 183000 MPa, and a density of $8x10^{-9}$ Mg/mm^3 was chosen for all foil configurations. Initially, a 140 MPa yield strength titanium material was used in an attempt to lower the overall weight of the hydrofoils. However, the titanium proved nowhere strong enough for the large forces seen by the outer extents of the foil at top speeds.

First Iteration Structural Analysis: Uniform Pressure Distribution

In the first iteration of the hydrofoil structural analysis, the load was treated as a uniform pressure and applied to the wetted area of the submerged hydrofoil. Three separate configurations of hydrofoils were analyzed and recommendations were made based on the findings.

Foil Configuration #1: No Support

For the first configuration, no supporting structure was added to the hydrofoil. The boundary conditions and loads were applied to the hydrofoil as mentioned in the previous sections and it was found that the maximum stress was approximately 603 MPa for the forward foil and 375 MPa for the aft foil. The stress fields for the forward and aft hydrofoil without supporting structure are shown in Figure 21 and Figure 22 below.

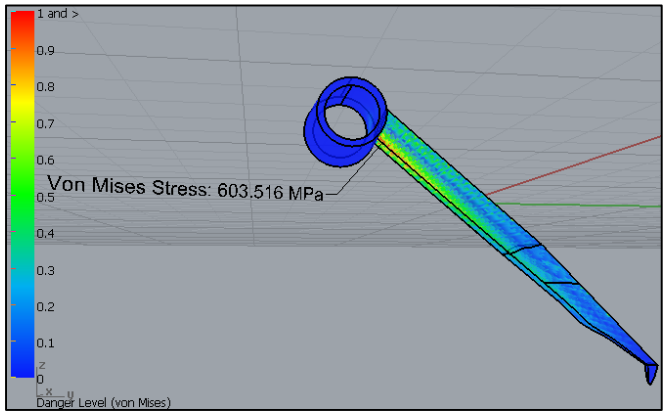

Figure 21: Forward Foil #1 Stress Field

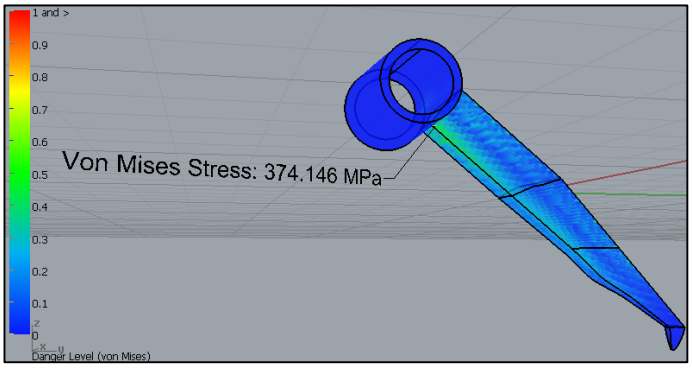

Figure 22: Aft Foil #1 Stress Field

In order to obtain an analytical comparison to the FEA results shown above, the hydrofoil was then approximated as a cantilevered beam and the maximum stresses were found from the equation:

$$\sigma_{max} = \frac{M_{max}}{S}$$

Where:

$M_{max} = F_{Total} * l$

$l =$ distance from support to center of force

$S = beam\ equivalent\ section\ modulus$

The maximum stresses found analytically were 520.5 MPa in the forward foil and 250.8 Mpa in the aft foil.

Foil Configuration #2: Strut Support

In the next configuration, a large strut was added to support the hydrofoil as seen in Figure 23. The sizing and placement of the strut was initially chosen by observing where the stress concentration areas were in the previous configuration, but after many iterations with the FEA tool the team was able to size and place a strut in a way that allowed for the least stress in the hydrofoil. The location of the lower strut arm was limited to the parallel section of the hydrofoil so that it would not interfere with the supercavitating flow during top speeds. After many design iterations on the forward hydrofoil, it was determined that placing the lower strut arm at a distance of 1.4 meters from the bottom of the parallel hydrofoil section provided enough support to keep the maximum stresses within the 2X yield stress safety factor. The aft strut arm was then placed at the same angle as the forward in an attempt to reduce the drag effects of the aft strut. This angle for the aft strut resulted in its placement of 50 millimeters above the bottom of the parallel hydrofoil section. The strut's cross section was shaped in a hydrodynamically efficient way so as to lower the added resistance from the strut during takeoff. Further studies could include an optimization of the strut's cross section shape to reduce the drag while keeping the strength benefits developed in this study.

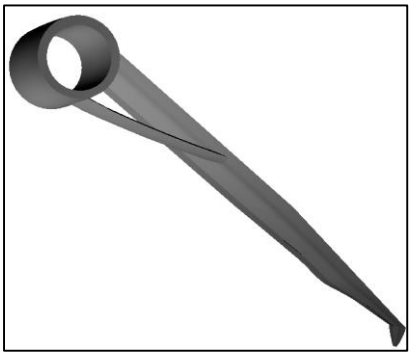

Figure 23: Front Hydrofoil with Supporting Strut

Once the loads were applied to the forward hydrofoil and the strut was resized appropriately, the maximum stresses found near the strut were around 300 MPa. However, there were three small 5 mm stress concentration areas on the leading edge of the foil that exceeded 1500 MPa. The design team believes these small stress concentrations are anomalies of the FEA program rather than physical stress concentrations due to the smooth nature of the foil. These stress concentrations were noted, but not taken into account during the strut sizing process. The stress field of the forward foil in this configuration is shown in Figure 24.

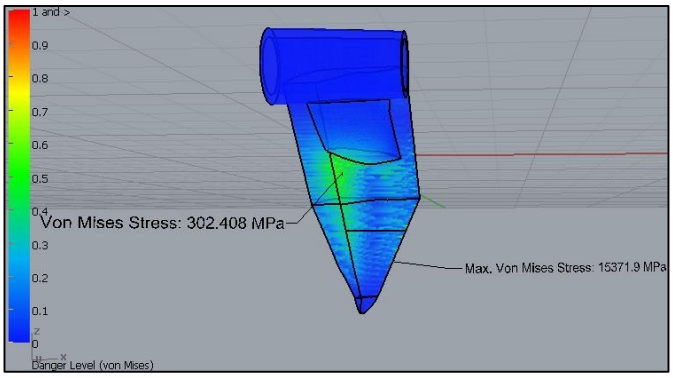

Figure 24: Forward Foil #2 Stress Field

The same approach used in the forward foil was used in sizing and placing the strut for the aft foil. After a few iterations, the maximum stress found near the aft strut was approximately 190 MPa. A single stress concentration of approximately 5 mm in diameter and over 2500 MPa was found on the leading edge of the aft hydrofoil, but was assumed to be an anomaly of the FEA program. An object as smooth as this hydrofoil could not physically have a 5 mm stress concentration on the edge of a large, flat plate. The stress field of the aft foil in this configuration is shown in Figure 25.

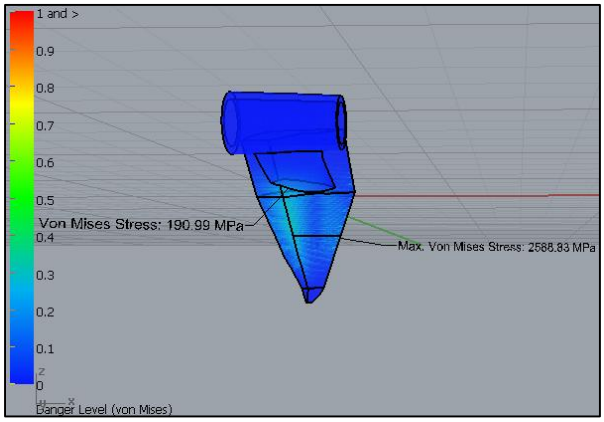

Figure 25: Aft Foil #2 Stress Field

The analytical comparison for the FEA results above used the same equations as in configuration #1, except in this calculation the strut was assumed to fully support the hydrofoil inboard of the strut. This effectively decreases the distance from the resultant force to the restraint, making the maximum moment much lower. The maximum stresses using this method were found to be 379.4 MPa in the forward foil and 225.3 MPa in the aft foil.

Foil Configuration #3: NACA 4412 Modification

In the final configuration, the parallel section of the hydrofoil was replaced by a NACA 4412 hydrofoil section of equal cord length. The NACA 4412 was chosen due to its proven performance in multiple model tests as well as its thick cross section for structural support. The NACA 4412 section was given a 4° angle of attack in order to provide a 0.8 lift coefficient, 0.02 drag coefficient and a proven low occurrence of cavitation below speeds of 30 kts (~52 f/s). The model test data for the NACA 4412 from reference [10] is given in Figure 26, Figure 27, and Figure 28 below.

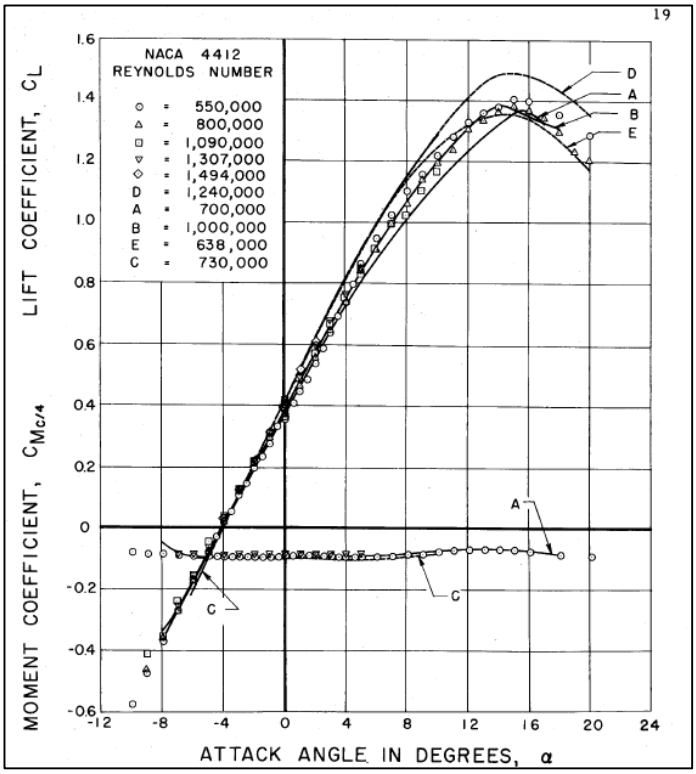

Figure 26: NACA 4412 Lift/Moment Coefficient vs Angle of Attack [10]

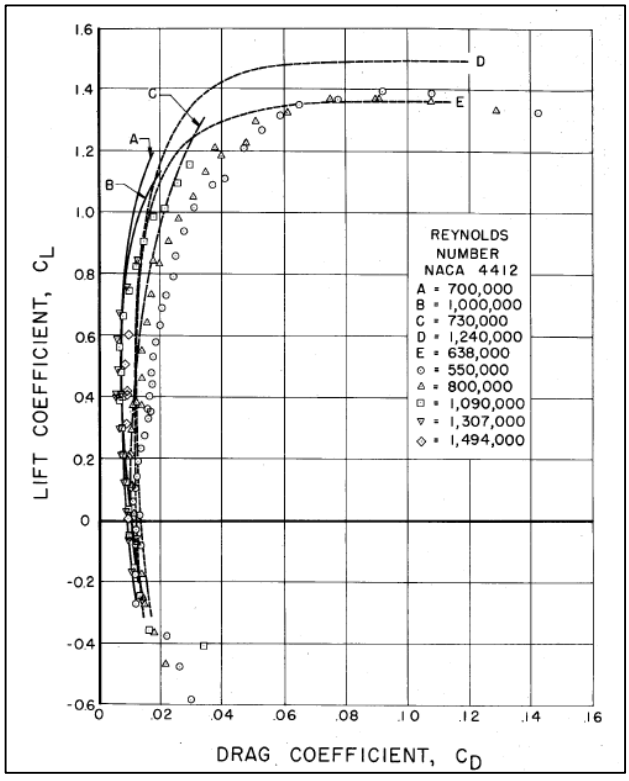

Figure 27: Lift vs Drag Coefficients [10]

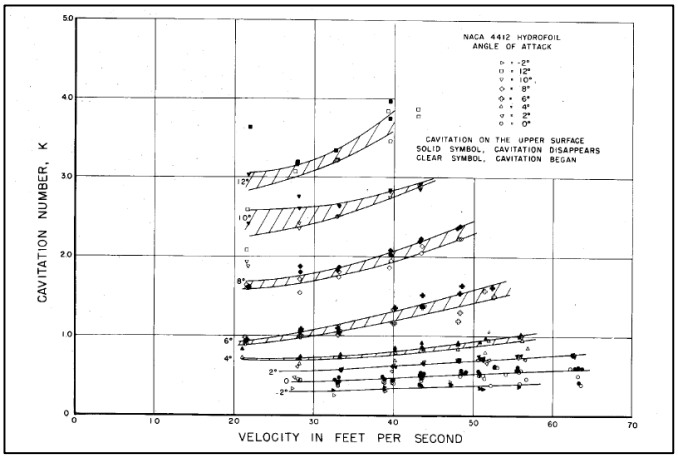

Figure 28: NACA 4412 Cavitation Number vs Velocity [10]

The two types of hydrofoils were then lofted together to ensure the super-cavitating section would be seen by the incoming flow at higher speeds. A transparent view of the parallel section is shown in Figure 29, followed by a full body plan view of the modified hydrofoil in Figure 30.

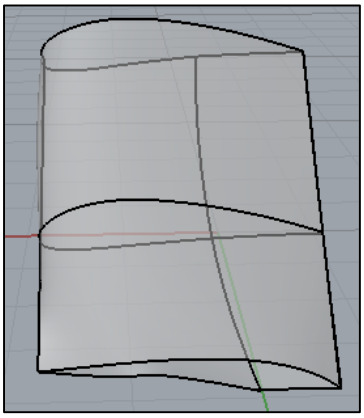

Figure 29: Mixed Hydrofoil Parallel Body Section

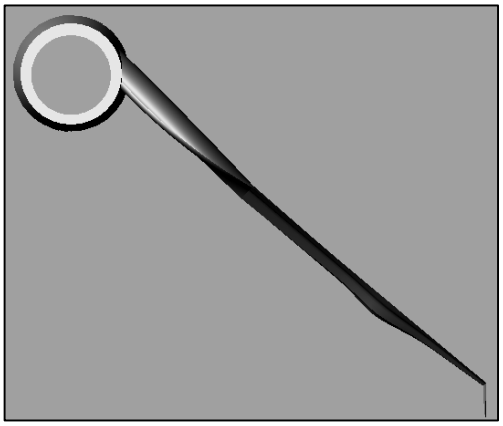

Figure 30: NACA 4412 Upper Section Modification, Body Plan View

The goal of this design configuration was to improve the structural adequacy of the hydrofoil while also improving hydrodynamic efficiency. Once it was determined that the hydrofoil would not be cavitating during the transition into foil borne mode, it occurred to the authors that it would be a good decision to use a sub-cavitating hydrofoil section in the inboard region of the hydrofoil. Not only would the thicker hydrofoil provide more structural stability than the thinner section, but it would also provide more lift than a super-cavitating hydrofoil would at those lower speeds. These facts, coupled with the loss of drag forces associated with adding a strut made the mixed type hydrofoil very appealing to the authors.

Once the hydrofoil was created, the same forces and restraints were applied as in the previous sections of this analysis. The average maximum stresses were 300 MPa for the forward foil and 190 MPa for the aft foil. Figure 31 and 32 show the stress fields of each foil.

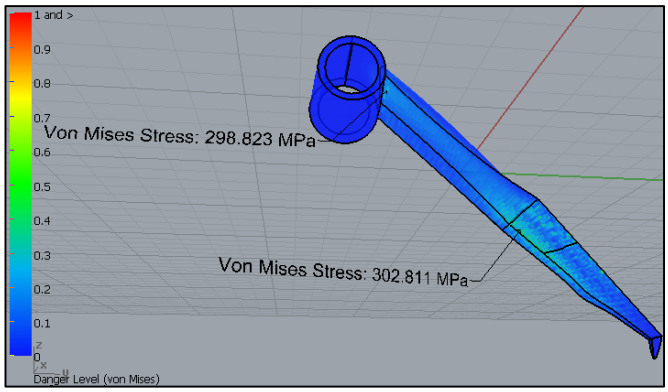

Figure 31: Forward Foil #4 Stress Field

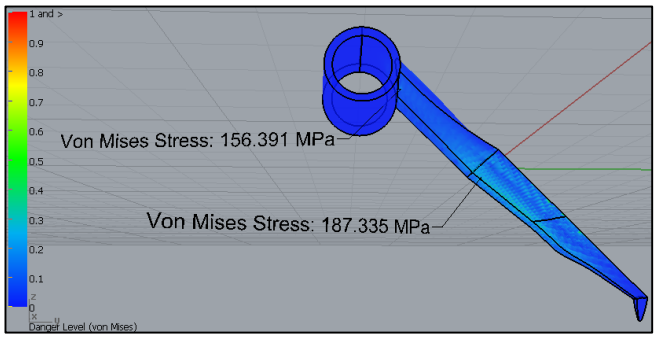

Figure 32: Aft Foil #4 Stress Field

To compare these FEA results to analytical calculations, the same equations as used in configuration 1 were used here. In this configuration however, the increased thickness of the NACA 4412 section greatly increases the section modulus of the foil, thereby decreasing the maximum stress to 382.4 MPa for the forward foil and 225 MPa for the aft foil.

Structural Analysis First Iteration Summary and Conclusion

For the 660 MPa tensile yield stress steel, both of the supporting types meet a 2x safety factor for the forward

foil and a 3x safety factor for the aft foil. A summary of the stresses found in this study for the different configurations is shown in Table 5.

Table 5: Structural Analysis Maximum Stress Summary

No Support	**Forward Foil**	**Aft Foil**
Analytical Max Stress (MPa)	659	317
FEA Max Stress, Avg (Mpa)	604	374
With Strut	**Forward Foil**	**Aft Foil**
Analytical Max Stress (MPa)	480	285
FEA Max Stress, Avg (Mpa)	302	190
With NACA Upper	**Forward Foil**	**Aft Foil**
Analytical Max Stress (MPa)	382	225
FEA Max Stress, Avg (Mpa)	300	180

Further tests should be conducted on the effects of changing from a subcavitating to supercavitating hydrofoil at mid-foil length. The design team believes the NACA support configuration to be the best. This configuration would be optimal for *Wavecutter* due to the vessel's slow speeds during transitioning into foil borne mode. The thicker upper section with the NACA 4412 profile allows for more structural stability than the thin supercavitating hydrofoil, eliminating the need for a strut support and thereby decreasing the overall drag force. The downside to adding the NACA 4412 is that it increases the weight by approximately 3% over the strutted configuration.

Structural Analysis Second Iteration: Computationally Determined Pressure Distribution

In the second iteration of the structural analysis, the force applied to the hydrofoil was altered in order to match the pressure distribution of the 2-dimensional (2D) computational fluid dynamics (CFD) results. The resulting deflections and stresses of each type of hydrofoil were analyzed and recommendations were made based on the results. All calculations shown in this section are for the forward foil only. The same process was used for the aft foil.

CFD Modelling

The pressure distribution along the wetted portion of the SC-SP hydrofoil was obtained from specific CFD simulations capitalizing on the expertise of Dr. Brizzolara [6] on the simulation of three multiphase viscous turbulent flows with the combined effect of cavitation and ventilation from the free surface. An example of the results obtained by CFD simulations is shown in Figure 33.

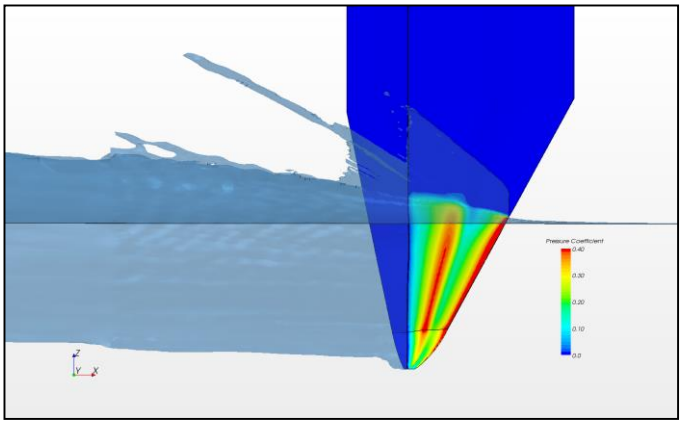

Figure 33: CFD pressure Distribution on face of the SC-SP hydrofoil. Dark blue: ventilated hydrofoil surface, light blue cavity and spray free surface

From these CFD results, the discrete pressure values calculated at the center of each cell face of the hydrofoil surface were interpolated with a polynomial function along the chord and a linear scaling factor along the span to develop a continuous equation estimate.

Creating a 3D pressure surface

The resulting 3-dimensional (3D) mathematical surface is an interpolation of the pressure distribution that spanned the wetted surface of the SC-SP hydrofoil. A visual representation of the 3D surface pressure distribution created for application onto the hydrofoil is shown in Figure 34.

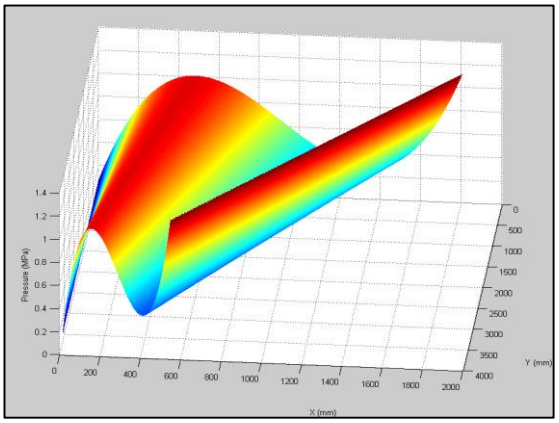

Figure 34: 3D CFD Pressure Interpolation

After the 3D equation was determined, it was imported to the FEA software for structural testing. A visual representation of the CFD pressures applied to the hydrofoil are given in Figure 35. Notice the consistency of the 2D CFD pressure curvature along the depth of the hydrofoil.

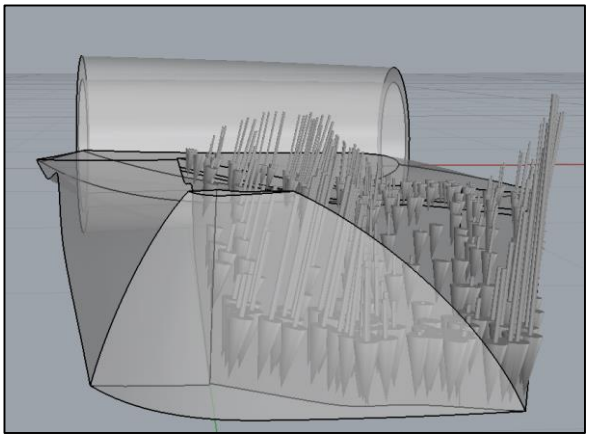

Figure 35: 3D Pressure Applied to the Hydrofoil

Strut vs NACA 4412 Support

The same structural analysis was conducted as in the first iteration, however this time the CFD pressures were applied to both the strut and NACA 4412 support versions of the hydrofoil. As seen in Figure 36 when the new pressures are applied to both versions of the forward hydrofoil, the strut supported version does not maintain the 2X safety factor. The new maximum stress in the forward foils is now 426 MPa for the strut version and 235 MPa for the NACA 4412 support version.

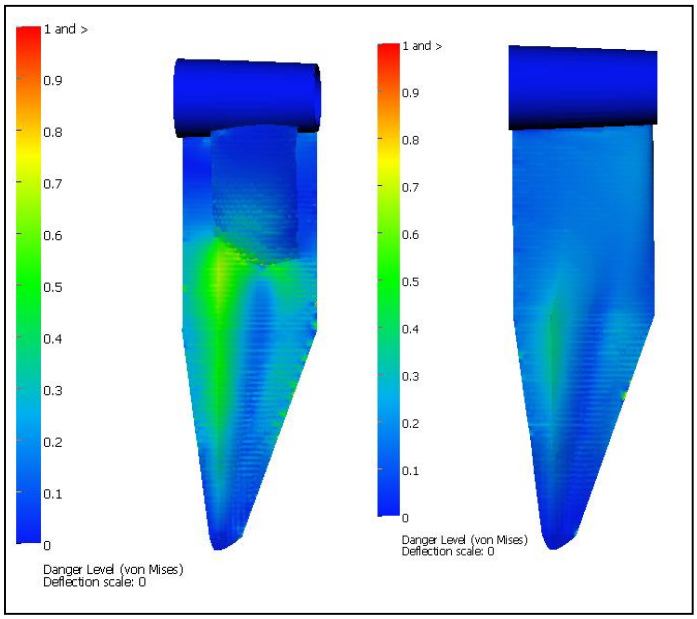

Figure 36: Forward Foil Strut Support (Left) and NACA 4412 Support (Right) Stress Distribution

From the above Figure, it is clear that if the strut support is chosen as the actual structural support configuration, then further design iterations should be conducted on the placement and sizing of the forward foil strut in order to ensure maximum effectiveness against various forces seen in the actual marine environment.

Structural Analysis Second Iteration Conclusions

The NACA 4412 structural configuration provided much lower stresses than the strut support under the design loading conditions as determined by CFD. It is also apparent from this analysis that the NACA 4412 is a more robust design than the strutted configuration due to its ability to withstand many different types of loading. The strutted configuration reduces the total bending moment seen within the foil from a uniformly applied load, but it does not perform well when the hydrofoil has the associated torsional stresses within it from the CFD loads. The NACA 4412 should be incorporated into future iterations of *Wavecutter* design.

FEASIBILITY ASSESSMENT

The feasibility assessment examines static stability and seakeeping of the vessel in foil borne mode, maximum speed (85 knots).

LONGITUDINAL STATIC STABILITY

Transverse stability is more or less guaranteed from the large lateral distance of the surface piercing hydrofoils. Longitudinal stability is not as apparent and thus is a priority in this preliminary design study. Positive static stability means that for a given pitch angle offset from the initial equilibrium state, the reaction moment must tend to return the vessel to its upright position. A program has been developed in Matlab® environment simulating an 'inclining experiment' for the vessel in foil-borne mode in the longitudinal/vertical plane. The output of the program is the righting arm moment generated at various consecutive pitch positions starting from an initial dynamic equilibrium condition.

During a typical inclining experiment, a moment is applied to the vessel by transferring weights. The result is a slow rotation and a heave position change. The latter occurs because vertical force equilibrium has to be satisfied. Each consecutive pitch position, in the inclining experiment simulation, is caused by a different moment applied. The resulting righting moment graph is seen in Figure 37. The moment is seen to be zero when pitch is zero, confirming that at zero pitch equilibrium occurs. This is a good validation that the program works properly, at least in the zero pitch condition. It can be seen that a negative reactive moment is produced in a positive pitch position. This indicates that the vessel has positive static stability.

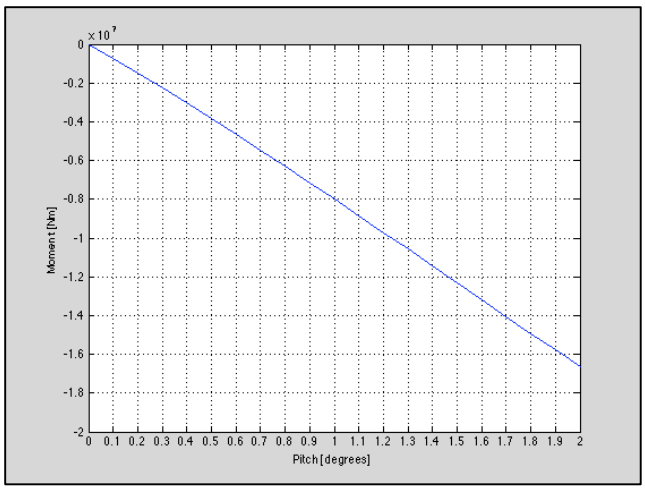

Figure 37: Righting Moment Graph for Small Angles

When the vessel changes pitch position, several forces change direction causing their moment with respect to the reference point to change. This effect has been considered in the calculation of the righting arm moment graphs. Each force is represented as a vector, applied at a specific point on the vessel. A rotational matrix is defined to incorporate the change in the point of application of the force vectors, as the vessel changes pitch position. Another matrix incorporates the change in heave position. Let $\vec{r}$ be the point of application of the the force $\vec{F}$ on the vessel.

$$\vec{r} = [r_x, r_z]$$
$$\vec{F} = [F_x, F_z]$$

$$Rot = \begin{bmatrix} \cos(pitch) & \sin(pitch) \\ -\sin(pitch) & \cos(pitch) \end{bmatrix}$$

$$Heave = [0, heave]$$
$$\vec{r}_{new} = \vec{r} * Rot + Heave$$

Some of the force vectors rotate with pitch and some do not. Hydrofoil forces already include the rotation element in the formulas, so they do not change direction with pitch motion. Weight vector also does not alter its direction with pitch. Air drag force components, thrust and wing lift do alter their direction with pitch. Apart from vector direction, all forces except weight also change in magnitude, in a different heave and pitch position. For each force, the resulting moment change from a random heave and pitch position is shown below.

$$\overrightarrow{\Delta M} = \vec{r}_{new} \times \vec{F}_{new} - \vec{r} \times \vec{F}$$

SEAKEEPING IN HEAD WAVES

Approach and assumptions

To assess the vessel's dynamic behavior in the vertical plane, the partially linearized differential equations of heave and pitch are defined and solved. In general, the dynamic responses of a vessel are an unsteady phenomenon, meaning that the parameters describing the phenomenon change with time, continuously. The simulations have been performed using a quasi-steady approach. In this respect, the hydrodynamic forces at each integration time step are updated and approximated with their value in steady condition. Diffraction damping is neglected for the hydrofoils while a constant added mass is considered. The system of differential equations are solved with numerical methods [11].

The seakeeping problem is simplified and solved with the superposition effect, by solving the wave excitation forces and hydrodynamic forces due to vessel motion independently. To estimate the first, the vessel is assumed to be still in terms of heave and pitch, while the incoming waves imposed forces on the vessel. The exciting forces are a result of the wave imposing a different submerged length and angle of attack to the foils, while the vessel is traveling at maximum speed. To estimate the hydrodynamic forces due to motions the sea is assumed calm and the vessel has a random heave & pitch position/velocity. The hydrodynamic forces are calculated with a quasi-steady approach as a function of heave, pitch instantaneous values and heave and pitch velocity. Radiation and diffraction forces that depend on heave and pitch velocities (damping forces) were not known, and no source could be found to give an estimation of them for super-cavitating hydrofoils. The only damping terms considered were the ones resulting from the change of hydrofoil lift due to the induced angle of attack by heave and pitch velocity, which result, in fact, in a highly dissipative contribution.

The assumptions that were made to derive the equations of motion are summarized below:

1. Heave added mass and pitch added mass moment of inertia of the hydrofoils are approximated using empirical formulas for a non-cavitating wing accelerating in a fluid [12]. All other terms in the added mass matrix are assumed zero. In addition added mass damping terms are neglected.
2. Free surfaces effects on added mass inertia and added mass damping terms are neglected for simplicity. In reality fully submerged versus partially submerged foils will have a difference in these terms.

3. Surge motion is considered uncoupled from heave and pitch. In reality there may be coupling involved with surge as well. Speed is considered to be fixed at 85 knots.
4. Foil interaction forces are neglected. The downwash of the front to the aft foil is ignored. However, the unsteady nature of foil interaction forces could be of significance in this problem. Computational fluid dynamics methods take into account these components, and this is one of the reasons why CFD seakeeping analysis is one of the recommendations for future work.
5. The effect of the history of the motions is neglected, otherwise named memory effects. While memory effects are not a major concern in sub-cavitating bodies, they can be important for super-cavitating bodies, because the shape and extent of the cavity depends on the history of motion [13]. Neglecting this effect is partially justified by the fact that the selected hydrofoil profile solves the unsteady ventilation problem that troubles many super-cavitating hydrofoil designs [6].
6. Some nonlinear wave force effects are neglected in the calculation of the external forces. Specifically the vessel is considered fixed as the wave progressed, thus the submerged foil geometry below the wave contour only depends of the wave profile. In reality, as the vessel performs heave and pitch motions, the external forces change not only due to the wave profile, but also due to the change in the submerged part of the foil below the wave contour.
7. The only damping terms included are the ones caused by the change in the flow angle of attack to the foils due to heave and pitch velocity. As previously mentioned, other damping terms could not be determined for super-cavitating hydrofoils.
8. Wave exciting Froude-Krylov forces and diffraction forces are assumed negligible, due to the small volume of the hydrofoils.

Equations of motions:
The generic equations of motion are derived from Newton's second law.

$$(M_{33} + A_{33}) * \ddot{\eta}_3 + \sum F_{3res}(\eta_3, \eta_5, \dot{\eta}_3, \dot{\eta}_5) = \sum F_{3ex}(t)$$
$$(I_{55} + A_{55}) * \ddot{\eta}_5 + \sum F_{5res}(\eta_3, \eta_5, \dot{\eta}_3, \dot{\eta}_5) = \sum F_{5ex}(t)$$

M_{33}: $vessel\ weight\ [kg]$
I_{55}: $vessel\ pitch\ mass\ moment\ of\ inetria\ [kg * m^2]$
A_{33}: $vessel\ heave\ added\ mass\ [kg]$
A_{55}: $vessel\ pitch\ added\ mass\ moment\ of\ inetria\ [kg * m^2]$
$\ddot{\eta}_3$: $heave\ acceleration\ [\frac{m}{s^2}]$
$\ddot{\eta}_5$: $pitch\ acceleration\ [\frac{rad}{s^2}]$
$\dot{\eta}_3$: $heave\ velocity\ [\frac{m}{s}]$
$\dot{\eta}_5$: $pitch\ velocity\ [\frac{rad}{s}]$
η_3: $heave\ position\ [m]$
η_5: $pitch\ position\ [rad]$

$\sum F_{3ext}$: $sum\ of\ all\ external\ forces\ [N]$
$\sum F_{5ext}$: $sum\ of\ all\ external\ moments\ [N * m]$
$\sum F_{3rad}$: $sum\ of\ all\ restoring\ forces\ [N]$
$\sum F_{5rad}$: $sum\ of\ all\ restoring\ moments\ [N * m]$

Inertia terms:
The inertia terms are calculated from the weight and the weight distribution of the vessel. The added mass inertia terms are estimated from Korotkin's formulas [12]. The resulting mass and mass moment of inertia are:

$$M_{33} = 2.5452 * 10^5\ kg$$
$$I_{55} = 423.045 * 10^5\ kg * m^2$$
$$A_{33} = 8.3 * 10^3\ kg$$
$$A_{55} = 207.74 * 10^4\ kg * m^2$$

The added mass components have been calculated for a sub-cavitating foil, because only formulas for sub-cavitating speeds could be found. It is noticed that the added mass components are only a small portion of the vessel's total inertia. Specifically:

$$\frac{A_{33}}{M_{33}} = 3.3\ \%$$
$$\frac{A_{55}}{I_{55}} = 4.9\ \%$$

Based on the above percentages, the added mass and added mass moment of inertia terms are not expected to play a significant role in determining the vessel's motion responses.

Restoring forces:
Restoring forces can be found by assuming a random heave and pitch position and calculating the total force and moment at this position as a function of heave and pitch. The same process used in the static stability

section was used here to estimate the heave force and pitch moment change resulting from forces other than the hydrofoils forces. To estimate the change in the hydrofoils forces, the changes in the submerged length and angle of attack have to be considered, due to a random heave and pitch position and velocity.

$$T_f = T_{f0} - \frac{\eta_3}{\sin(40)} - \frac{LBF}{2} * \frac{\tan(\eta_5)}{\sin(40)}, for\ small\ angles\ \tan(\eta_5) \cong \eta_5$$

$$T_\alpha = T_{\alpha 0} - \frac{\eta_3}{\sin(40)} + \frac{LBF}{2} * \frac{\tan(\eta_5)}{\sin(40)}$$

$$p_f = p_{f0} + \eta_5 + tan^{-1}\left(\frac{\dot{\eta}_3 + \dot{\eta}_5 * \frac{LBF}{2} * \cos(\eta_5)}{V_{ship}}\right)$$

$$p_a = p_{a0} + \eta_5 + tan^{-1}\left(\frac{\dot{\eta}_3 - \dot{\eta}_5 * \frac{LBF}{2} * \cos(\eta_5)}{V_{ship}}\right)$$

$T_{f0}: front\ foil\ sub.\ length: equilibrium\ condition\ [m]$
$T_{a0}: aft\ foil\ sub.\ length: equilibrium\ condition\ [m]$
$T_f: front\ foil\ instant\ ub. length\ [m]$
$T_a: aft\ foil\ instant\ sub. length\ [m]$
$p_{f0}: front\ foil\ pitch\ equivalent\ angle\ of\ attack - equilibrium\ condition\ [rad]$
$p_{a0}: aft\ foil\ pitch\ equivalent\ angle\ of\ attack - equilibrium\ condition\ [rad]$
$p_f: front\ foil\ instant\ p.e. angle\ of\ attack\ [rad]$
$p_a: aft\ foil\ instant\ p.e. angle\ of\ attack\ [rad]$
$LBF: length\ between\ foils\ [m]$

The pitch-equivalent angle of attack is related to the angle of attack through the following geometric relationship.

$$p = a/\sin(dihedral\ angle)$$

$p: pitch\ equivalent\ angle\ of\ attack$
$a: angle\ of\ attack$

Notice that the foil lift and drag in Figure 14 do not change direction. This is due to the fact that the experimental formulas already consider angle of attack influence in lift and drag, both in coefficient and due to direction change of the vectors. In the formulas below, the force and moment change due to lift and drag are shown.

$$F_{foils} = 2 * q * \left([CF_{zf} * A_f - CF_{zf0} * A_{f0}] + [CF_{za} * A_a - CF_{za0} * A_{a0}]\right)$$

$$M_{foils} = 2 * q * \left(\frac{LBF}{2}\right) * \left([CF_{zf} * A_f - CF_{zf0} * A_{f0}] - [CF_{za} * A_a - CF_{za0} * A_{a0}]\right)$$

$F_{foils}: hydrofoil\ force\ change\ [N]$
$M_{foils}: hydrofoil\ moment\ change\ [Nm]$
$CF_{zf} = f(T_f, p_f)\ , lift\ force\ coefficient\ front\ foil$
$CF_{za} = f(T_a, p_a)\ , lift\ force\ coefficient\ aft\ foil$
$A_f = f(T_f)\ , sub. area\ front\ foil\ [m^2]$
$A_a = f(T_a)\ , sub. area\ aft\ foil\ [m^2]$
$CF_{zf0} = f(T_{f0}, p_{f0})\ , lift\ force\ coefficient\ front\ foil\ in\ equilibrium\ condition$
$CF_{za0} = f(T_{a0}, p_{a0})\ , lift\ force\ coefficient\ aft\ foil\ in\ equilibrium\ condition$
$A_{f0} = f(T_{f0})\ , sub. area\ front\ foil\ in\ equilibrium\ condition\ [m^2]$
$A_{a0} = f(T_{a0})\ , sub. area\ aft\ foil\ in\ equilibrium\ condition\ [m^2]$

$$q = \frac{1}{2} * \rho * Vship^2\ , coefficient\ [kg/(m^2 * s)]$$

$\rho: water\ density\ \left[\frac{kg}{m^3}\right]$
$Vship: vessel\ speed\ [\frac{m}{s}]$

The final formulas of heave restoring force and pitch restoring moment are not presented here, because each is approximately 4 pages long. The formulas are highly non-linear and both contain all terms of pitch, heave, pitch velocity and heave velocity.

External forces

External forces caused by head waves are examined in this study. Three different cases of wave length are examined, two of which represent the worst potential situations. The first is for a wave length of twice the length between front and aft hydrofoils (LBF). The second is for a wave length equal to the length between front and aft hydrofoils (LBF). The third is for a wave length corresponding to the most probable encounter period for the Gulf of Mexico [1]. The first two cases are shown in the two Figures 39 and 40, where sketches of the vessel encountering the waves have been made. It is obvious that the first wave length is expected to generate the largest possible moment, while the second to generate the largest possible heave force.

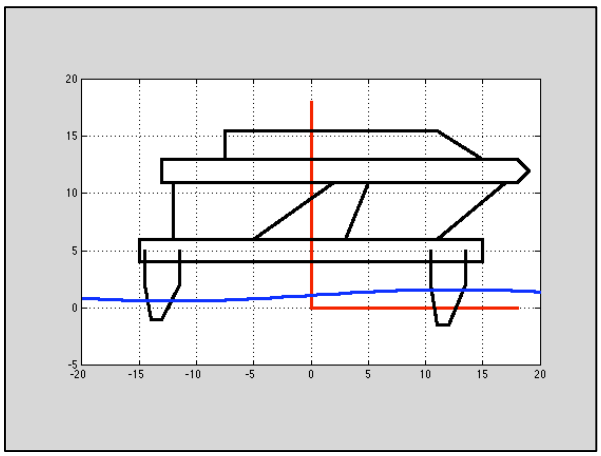

Figure 38: Wave Length Twice LBF

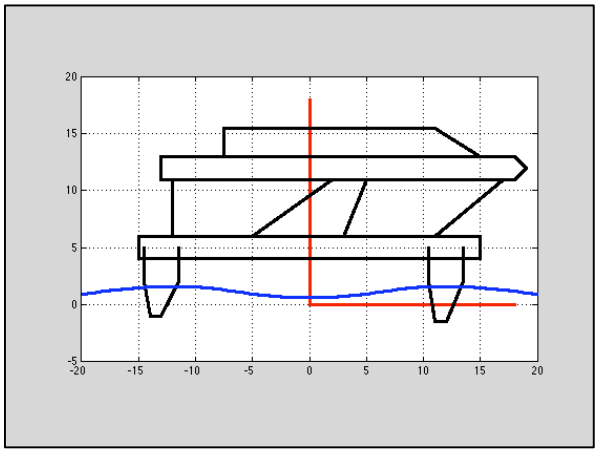

Figure 39: Wave Length Equals LBF

The external forces are due to the imposed change in submerged length and angle of attack, by the wave to the hydrofoils.

$$T_f = T_{f0} + \frac{zeta\ (xf)}{\sin(40)}$$
$$T_\alpha = T_{\alpha 0} + \frac{zeta\ (xa)}{\sin(40)}$$

$zeta\ (xf)$: $wave\ elevation\ at\ front\ foil$
$zeta\ (xa)$: $wave\ elevation\ at\ aft\ foil$

$$p_f = p_{f0} + tan^{-1}\left(\frac{w(xf,zf)}{u(xf,zf)}\right)$$
$$p_a = p_{a0} + tan^{-1}\left(\frac{w(xa,za)}{u(xa,za)}\right)$$

u: $horizontal\ flow\ velocity\ [\frac{m}{s}]$
$(includes\ the\ vessel's\ forward\ speed\ of\ 85\ knots)$
w: $vertical\ flow\ velocity\ [\frac{m}{s}]$

The incoming wave had the following equation:

$$\zeta = Re\{A * e^{(i*(k*x+\omega_{enc}*t+phase))}\}$$

Where
ζ: $wave\ elevation\ [m]$
A: $wave\ amplitude\ [m]$
ω_{enc}: $encounter\ frequency\ [\frac{rad}{s}]$
$phase$: $phase\ delay\ or\ advance\ [rad]$
x: $longitudinal\ axis\ coordinate\ [m]$
t: $time\ [s]$

Simulation results

Before imposing external forces to the system, a simulation has been performed with no external forces, but with initial conditions. This simulation serves to validate the results of the static stability analysis, as well as to observe the natural frequency of the system. The initial conditions are a heave of 0.5 m and a pitch of 2^0. The results of this simulation are in Figure 40. The vessel oscillates with its natural frequency. After approximately 4 natural periods, the vessel returns to its equilibrium position. Damping is due to the dissipative terms containing the change in angle of attack due to heave and pitch velocities. As mentioned in the assumptions, this is the only form of damping considered, but it seems to have a great contribution to the vessel's dynamic behavior.

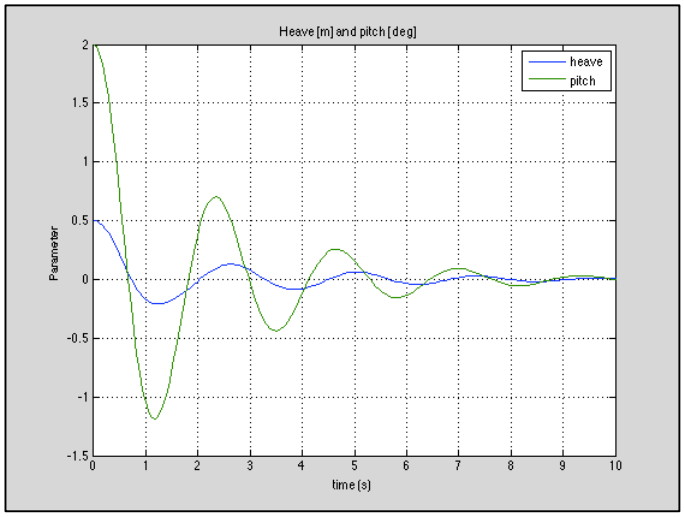

Figure 40: Simulation 1: Calm Sea with Initial Conditions

The findings reveal that the worst case of wave length is twice LBF (first case of external forces), because it results in the worst response motions. For this reason the second case of external forces is not presented in this paper. The motion responses for a wave height of 1.0 m are seen in Figure 41.

The input to the system is essentially a combination of an impulse and a sinusoidal input, because the wave is encountered suddenly, without a gradual increase or initial conditions. It can be seen in the graph that there are secondary peaks, before the system reaches a stable oscillation for both motions. These peaks are due to the impulse created by the sudden encounter of the wave. The heave amplitude is not significant, compared to the wave height. As expected, the pitch amplitude is noticeable, because this wave length is the worst in terms of pitch exciting moment. The period for both heave and pitch motion is seen ~0.9 s, which matches the encounter period of the wave. With this encounter frequency, issues regarding human safety and performance may arise, something which requires further consideration and study.

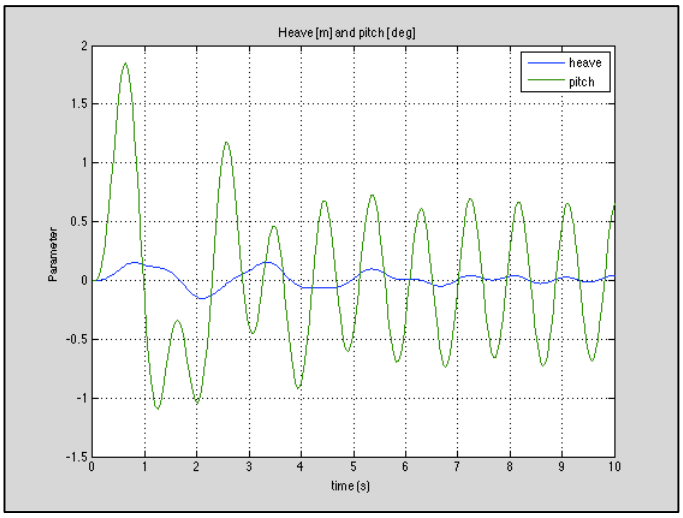

Figure 41: Simulation 2: Wave Length Twice LBF, Regular Wave Amplitude 0.5 m

While the motion responses seen above are for the worst possible wave length, they are not for the worst sea state. The highest operational sea state required for the vessel is the upper bound of sea state 4, per Table 1. This corresponds to a wave height of 2.5 m, thus a wave amplitude of 1.25 m. The motion responses for this wave amplitude are presented in Figure 42, which is the worst possible situation for the vessel. Just like in the previous simulation, motion secondary peaks are noticed upon encounter of the wave. Unlike in the previous simulations, oscillation of heave and pitch in steady state seems to occur around a non-zero value. This is explained by the fact that in this wave height, the parallel part of the foil enters the water level, contributing in a different way to the restoring and external forces. The average of the external forces in a wave period is different than the equilibrium lift forces, because of the unsymmetrical shape of the hydrofoil itself with respect to the equilibrium water level plane. The important conclusion of this simulation is that in the steady state phase, motion responses are stable and with small amplitudes relative to the incoming wave.

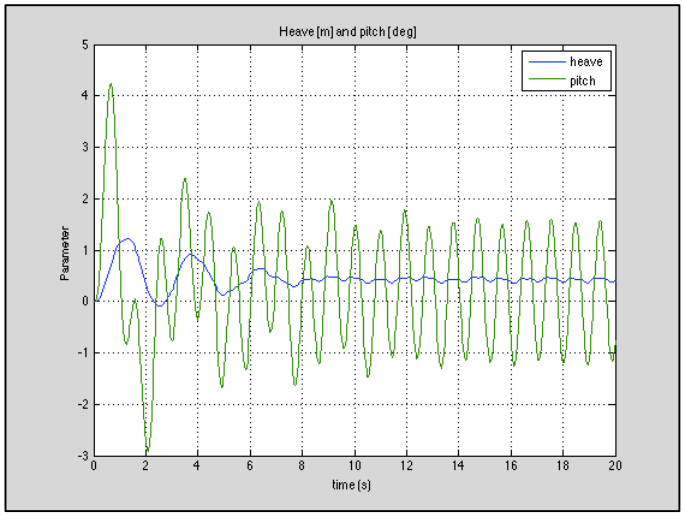

Figure 42: Simulation 3: Wave Length Twice LBF, Regular Wave Amplitude 1.25 m

The last simulation that has been performed corresponds to the most probable wave period in the Gulf of Mexico, for the sea state 4 upper bound. The most probable wave period in the Gulf Mexico is 4.9 s [1], which corresponds to a wave length of 37.5 m. The results of this simulation are shown in Figure 43. The motion responses indicate stable oscillation and acceptable seakeeping behavior.

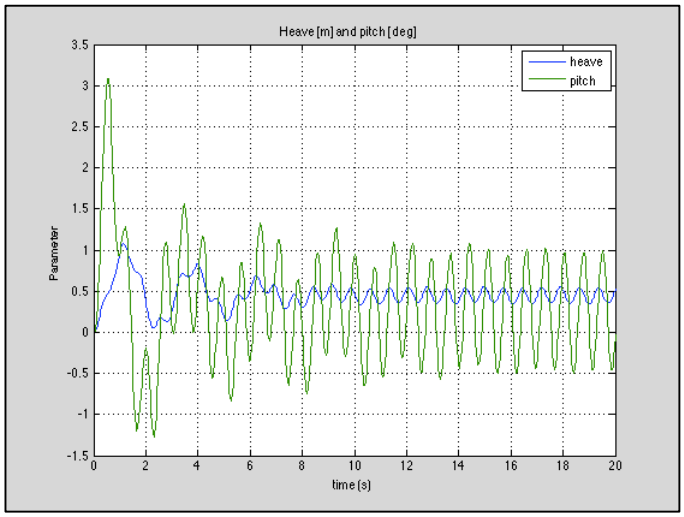

Figure 43: Wave Length 37.5 m (most probable in Gulf of Mexico), Regular Wave Amplitude 1.25 m

CONCLUSIONS AND RECOMMENDATIONS

This study results in an innovative hybrid hydrofoil/SWATH high speed vessel, with the intended mission of rapid transportation of crew and cargo. The design builds on Brizzolara's unmanned high speed hybrid hydrofoil/SWATH vessel [2]. The design is expanding the borders of the family of unconventional SWATH vessels of Brizzolara and Chryssostomidis, by including manned vessel to this family [14]. The general design phase focuses on the integration of the manned module, internal arrangements, weight estimation, speed profile determination and engine selection. The main characteristics of the vessel are seen below.

Table 6: Wavecutter Main Characteristics

Weight [MT]	254.52
Maximum speed [knots]	85
Required power at maximum speed [KW]	21140
Passenger capacity [people]	24
Crew size [people]	4
Cargo capacity [MT]	15
Endurance [NM]	480

With the above capabilities, *Wavecutter* has been placed on the Gabrielli-von Karman graph, shown in Figure 44, in order to evaluate its feasibility in terms of transport efficiency. The following are noticed from this figure:

- *Wavecutter* achieves a higher speed than vessels with the same specific power. Thus it is more efficient than these vessels.
- *Wavecutter* achieves 85 knots, with a lower specific power than vessels of equal speed. Thus it is more efficient than these vessels as well.

The high speeds of this vessel dictated the use of a super-cavitating hydrofoil. The specific hydrofoil profile was selected because of its ability to retain steady ventilation even under unsteady flow conditions [6]. The final sizing of the hydrofoils is

1. Front foil total length=8.7 m
2. Aft foil total length=8 m

Due the long, thin shape of the chosen super-cavitating (SC) surface-piercing hydrofoils and the severe loading imposed on the hydrofoils, a comprehensive structural analysis was performed. The results of the structural analysis indicated that structural support is necessary and two options were evaluated. The preferred option is a SC section blended with a partial NACA 4412 section. The NACA 4412 support option proved to be a more robust design than the strutted configuration due to its ability to withstand many different types of loading. In particular, the strutted configuration does not respond well to torsional loads, which were confirmed to be present from the CFD simulation.

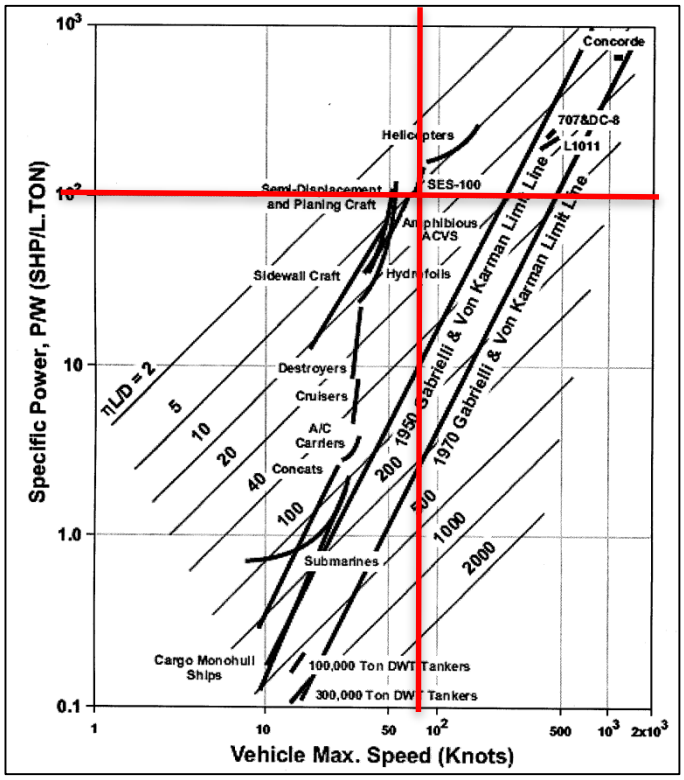

Figure 44: Gabrielli-Von Karman graph of transport efficiency

Static stability findings confirm the inherent stability of the hydrofoil configuration adopted (surface piercing foils with negative dihedral angle). Seakeeping analysis findings indicate a good seaworthiness in foil borne mode, at least up to a high sea state 4. However, issues regarding the human factor may be of concern, due to the high frequency of the response motions, for high wave encounter frequencies. A more detailed study should eventually include prediction of vertical accelerations in irregular waves and calculation of the Motion Sickness Incidence (MSI) and other human performance operability criteria.

The dynamic response findings of this study are not inclusive of all potential external disturbances that may occur. For example, motion responses due to high speed turning, various maneuvers and waves of incident angle other than the one of head waves are very important and should become the focus of future work. The results of the seakeeping analysis are summarized in Table 7. The

magnitudes of heave and pitch response in the table correspond to the amplitude of oscillation in the steady state phase of system response.

Table 7: Seakeeping Simulation Summary of Results

Wave height [m]	Wave length [m]	Time to reach steady state [s]	Approximate heave amplitude at steady state [m]	Approximate pitch amplitude at steady state [deg]
1.0	49.14	~8	0.05	0.65
1.0	24.57	~9	0.05	0.045
2.5	49.14	~17	0.1	1.2
2.5	24.57	~13	0.1	0.5
2.5	37.5	~16	0.1	0.75

REFERENCES

[1] Lumb, F.E., and N. Hogben. *Ocean Wave Statistics*. London: Ministry of Technology, National Physical Laboratory, 1967.

[2] Brizzolara S. (2011). Hydrodynamic Design and Assessment by CFD Methods of a Hybrid Hydrofoil / SWATH hull for a Super High Speed USV. ONRG-N62909-10-1-7116 final report, Office of Naval Research Global, US Navy.

[3] Brizzolara S. (2004) Parametric Optimization of SWAT-Hull Forms by a Viscous-Inviscid Free Surface Method Driven by a Differential Evolution Algorithm. Proceedings 25th Symposium on Naval Hydrodynamics, St. John‟s, Newfoundland and Labrador, vol. V, 47-64.

[4] Hochbaum, A.C., and C. Eckl. *Forces on a Super-Cavitating Hydrofoil*. Department of Dynamics of Maritime Systems. Berlin: Technische Universitat Berlin, 2012.

[5] Hoerner, S.F. *Fluid-Dynamic Drag*. Great Britain: L.A. Hoerner, 1992.

[6] Brizzolara S. (2013). Super-cavitating (SC) Surface-Piercing (SP) Hydrofoils: Design and Optimization Methods. ONRG-N62909-11-1-7007 final report. Office of Naval Research Global, US Navy.

[7] Vernengo G., Brizzolara S. (2012). A Reformulated Lifting Line Theory for Supercavitating Hydrofoil Design. Proceedings of the Eighth International Symposium on Cavitation (CAV 2012). Research Publishing Services. ISBN: 978-981-07-2826-7, doi:10.3850/978-981-07-2826-7 281.

[8] Martin Engineering Company, Baltimore Division "Hydrofoil Ship Structural Design Criteria Study." Report to the Bureau of Ships under contract Nobs-4791. Delivered September 8, 1965.

[9] Scan & Solve™ for Rhino. 2014. http://www.intact-solutitions.com/sns_documents/sns_v1/index.htm (accessed May 8, 2014).

[10] Kermeen, Robert W. *NACA 4412 and Walchner Profile 7 Hydrofoils in Noncavitating and Cavitating Flows*. Report No. 47-5, Bureau of Ships Fundamental Hydromechanics Research Program, 1956.

[11] Tearle, Matt. (2011) Solving ODEs http://www.mathworks.com/academia/student_center/tutorials/computational-math/solving-ordinary-diff-equations/player.html

[12] Korotkin, A. I. Added Mass of Ship Structures. St. Petersburg: Krylov Shipbuilding Research Institute, 2007.

[13] Uhlman, J., et al. Calculation of the Added Mass and Damping Forces on Supercavitating Bodies. *Fourth International Symposium on Cavitation*. Pasadena, CA, USA: California Institute of Technology, 2001.

[14] Brizzolara, S., and C. Chryssostomidis. The Second Generation of Unmanned Surface Vehicles: Design Features and Performance Predictions by Numerical Simulations. *ASNE Day 2013*. Arlington, VA, 2013.

ACKNOWLEDGMENTS

This design project owes its completion to Dr. Stefano Brizzolara, Director of the MIT i-Ship lab. His enthusiasm and knowledge of hydrofoils and Naval Architecture in general gave valuable insight to the design team.

AUTHOR BIOGRAPHIES

LTJG Vasileios Georgiadis, HN:

Vasileios has been an engineering duty officer for the Hellenic Navy ever since he graduated from the Hellenic Naval Academy in June 2006. Between graduation and June 2011, he has served mostly onboard MEKO-type frigates, his last position being the Head of the Electrical and Automations department. Since June 2011, he has been studying in the Massachusetts Institute of Technology. He has recently completed his studies, earning a Naval Engineer's Degree, a Master of Science in Mechanical Engineering and Master of Science in Engineering and Management.

LT Kyle Miller, USN:

Kyle graduated from the U.S. Naval Academy in May 2008, earning a B.S. in Systems Engineering. After receiving his commission, he served onboard USS ROOSEVELT (DDG-80) as the Gunnery Officer. LT Miller transferred into the Engineering Duty Officer community in 2010, where he was assigned to the Southeast Regional Maintenance Center and CNSL CRUDES, Mayport, FL. In April 2011, he began his postgraduate studies at the Massachusetts Institute of Technology. In June 2014, he will graduate from the Naval Construction and Engineering Program earning a Naval Engineer's Degree and a Master of Science in Mechanical Engineering.

LT Leon Faison, USN:

Leon graduated from Christian Brothers University in June 2007 earning a B.S. in Electrical Engineering. After receiving his commission in the ROTC program at the University of Memphis, he reported onboard USS VICKSBURG (CG-69) as the Communications Officer. After executing his option to transfer into the Engineering Duty Officer community, LT Faison was accepted to the Marine Engineer Diving Officer course at the Naval Diving and Salvage Training Center. In June 2014, he will graduate from the Naval Construction and Engineering Program earning a Naval Engineer's Degree and a Master of Science in Mechanical Engineering.